An STM Investigation of Sulfur and Alkoxide Adsorption on Ni(100)

Ali R. Alemozafar and Robert J. Madix*

Department of Chemical Enineering, Stanford University, Stanford, California 94305-5025

Received: January 19, 2005

The effect of sulfur on alkoxide formation and decomposition on the Ni(100) surface has been investigated with STM and LEED. At low coverage sulfur adsorbs into a p(2 × 2) structure, in agreement with LEED measurements and previous STM results. With increasing sulfur coverage, the p(2 × 2) structure saturates the surface and scattered domains of c(2 × 2) appear. Further increases in sulfur coverage affect increases in c(2 × 2) domain sizes; the state of the sulfur-covered surface up to 0.43 ML is characterized by p(2 × 2) and c(2 × 2) domains. STM measurements of the evolution of the sulfur-covered surface with $D_2S(g)$ adsorption are suggestive of sulfur nucleation and growth at multiple sites on the surface. Alkoxide formation on these surfaces was studied following exposure to ROH (R = CH_3, CH_3CH_2, $CH_3CH_2CH_2$, and C_6H_5). The alkoxy surface intermediates adsorbed in p(2 × 2)-S vacancies and, in the case of phenoxy, between hollow sites. Agreement between the methoxy coverage determined by XPS and the fraction of the surface covered with p(2 × 2)-S, as determined by STM, suggests that the p(2 × 2) vacancies are the sites of methoxy adsorption, and hence the active sites for selective poisoning.

A. Introduction

The interaction between sulfur and various metal surfaces has been the subject of numerous investigations. Our studies are motivated by the intent to gain a better understanding of how sulfur affects the catalytic activity of various metal surfaces. Of particular interest is Ni for its utility in methanation catalysts.

On Ni(110) and Cu(110) sulfur adsorbs into domains of a c(2 × 2) structure that grow and saturate the surface.[1,2] Domain boundaries, the product of a mismatch between separate sulfur islands, are characteristic of the structure on both surfaces. On Cu(110) at higher sulfur coverages, the p(5 × 2) and p(8 × 2) surface structures appear sequentially in order of increasing sulfur coverage.[2]

The adsorption of sulfur on the Ni(100) surface has been probed with an array of surface analytical instruments, among which are low energy electron diffraction (LEED),[3] polarization-dependent surface extended X-ray absorption fine structure spectroscopy,[4] and LEED IV[5]— all of which have enabled a better understanding of the structural and electronic properties of the system. LEED IV measurements were used to determine the 4-fold hollow binding site of sulfur on the Ni(100) surface.[5]

A scanning tunneling microscopy (STM) investigation of sulfur on Ni(100) by Leibsle and co-workers resolved the p(2 × 2)-S structure.[6] With increasing sulfur coverage, bright regions within a p(2 × 2)-S covered surface were ascribed to domains of c(2 × 2)-S, an assignment that was made to explain the c(2 × 2) LEED pattern, though the atomic arrangement within this structure was not directly imaged by STM. A follow-up STM investigation into the influence of sulfur on the oxidation of the Ni(100) surface showed oxide nucleation to occur primarily at step edges.[7]

Apart from its poisoning effects, sulfur has been shown to change the selectivity of surface-mediated processes. One particular case is the reaction of methanol (CH_3OH) on the Ni(100) surface.[8] On clean Ni(100) methanol reacts to form a methoxy (CH_3O−) surface intermediate, which completely dehydrogenates into CO(g) and H_2(g) with heating (Figure 1a).

$$CH_3O(a) \rightarrow CO(g) + 3/2\ H_2(g) \quad \text{[complete dehydrogenation]} \quad (1)$$

Preadsorbed sulfur on the surface leads to the partial dehydrogenation of the methoxy intermediate to give formaldehyde (H_2CO) and H_2(g) (Figure 1b):

$$CH_3O(a) \rightarrow H_2CO(g) + {}^1/_2H_2(g) \quad [\theta_s > 0.25\ \text{ML; partial dehydrogenation}] \quad (2)$$

The selectivity toward partial dehydrogenation increases with sulfur coverage, maximizing at coverages between 0.25 and 0.35 ML.[9] The spatial distribution of sulfur that affects the optimum yield of formaldehyde was suggested to consist of equal proportions of the p(2 × 2) and c(2 × 2) structures on the basis of the dependence of the yield of H_2CO on sulfur coverage.

In subsequent work the reactivity of ethanol and 2-propanol with the sulfur-covered Ni(100) surface was probed.[10] At low sulfur coverages total dehydrogeneation dominates the reaction of the alkoxy surface intermediate. With increasing sulfur coverage, formation of aldehydes was enhanced at the expense of CO and H_2; methane was not observed. It was concluded that alkoxy intermediates formed via dehydrogenation and that their decomposition to CO, H(a), and C(a) with heating was limited by adsorbed sulfur due to the increased activation barrier for C−H bond activation.

The adsorption of CO on the sulfur-covered Ni(100) surface has been used to probe available binding sites for the alkoxy. Using high-resolution electron energy loss (vibrational) spectroscopy (HREELS), Gland et al. showed that CO binds in 4-fold hollow and bridge sites in the p(2 × 2) structure.[11] With increasing sulfur coverage, the binding site shifts to 4-fold hollows amid sulfur in a c(2 × 2) configuration. A follow-up study with infrared spectroscopy (FTIR) and TPD showed that at low to moderate sulfur coverages the distribution of CO is

10.1021/jp050338l CCC: $30.25
Published on Web 05/12/2005

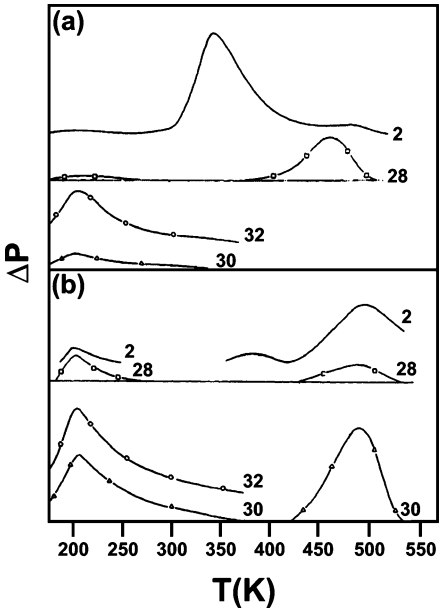

Figure 1. TPR spectra adapted from ref 9, showing the evolution of selected masses with temperature following (a) a saturation dose of CH_3OH on a clean Ni(100) surface at 159 K and (b) a saturation dose of CH_3OH at 159 K on Ni(100) precovered with 0.31 ML sulfur.

inhomogeneous and the desorption kinetics of CO are markedly affected by the initial state of the adlayer.[12] At higher sulfur coverages, inhomogeneities in the sulfur adlayer lead to isolation of adsorbed CO.

The bonding as well as the mechanism and kinetics of methoxy decomposition on Ni(100) was examined with time-resolved Fourier transform infrared spectroscopy (TR-FTIR).[14] At low coverage, methoxy orients with its C−O bond nearly normal to the surface, giving the alkoxy C_s symmetry.[13] The orientation was uninfluenced by preadsorbed sulfur, even though the amount of methoxy formed from methanol was significantly reduced. The activation energy of methoxy decomposition to CO and hydrogen was found to increase by about 1 kcal/mol upon adsorption of 0.14 ML of sulfur on the clean surface, which suggests that sulfur stabilizes the methoxy surface intermediate.

In this paper the results of an STM investigation of sulfur on Ni(100) and its effect on alkoxide binding are presented. At low coverage sulfur adsorbs in domains of a p(2 × 2) structure separated by patches of the clean surface. With increasing sulfur coverage this covers the entire surface, but defects such as domain boundaries, vacancies, and scattered moieties of sulfur in a c(2 × 2) arrangement appear. As the sulfur coverage is further increased, domains of the c(2 × 2) structure grow in size. The alkoxides formed from ROH (R = CH_3-, CH_3CH_2-, $CH_3CH_2CH_2-$, C_6H_5-, $CH_2{=}CH-CH_2-$) on the sulfur-covered Ni(100) surface at a sulfur coverage near 0.25 ML occupy p(2 × 2) vacancies, which thus appear to be the active sites for the partial dehydrogenation of the alkoxy surface intermediates.

B. Experimental Section

Experiments were performed in an ultrahigh vacuum chamber equipped with STM, low energy electron diffraction (LEED, OCI), Auger electron spectroscopy (AES, OCI), and a quadrupole mass spectrometer (QMS, Balzers) for temperature programmed reaction spectroscopy (TPRS) measurements. The chamber was also equipped with a sputter ion gun and stainless steel gas dosers. The system exhibited a base pressure of 2 × 10^{-10} Torr.

The STM employed in this study was of the "Johnnie Walker" type with RHK STM 100 control electronics.[15] The Pt/Ir tip was prepared by induced field evaporation onto a gold foil (∼3.9 μA, 15 min) in situ prior to STM measurements. Scan dimensions were calibrated with use of the Ni(110)-p(2 × 1)-O structure.[16]

The Ni(100) crystal used in this study had been bulk cleaned and used previously.[9] The day-to-day cleaning procedure consisted of two Ar^+ sputter (500 eV, 1.5−2 μA, 300−500 K, 10 min) and anneal (1050 K, 10 min) cycles. This procedure gave a surface devoid of all impurities detectible by AES but carbon, which was titrated away by cleaning cycles that consisted of low oxygen exposure at room temperature, heating to 600 K, and hydrogen treatment at 600 K to remove residual oxygen. This procedure was followed by a final sputtering and annealing cycle. A sharp p(1 × 1) LEED pattern was obtained following this cleaning procedure, indicative of a well-ordered surface. Within detection limits, AES showed the surface to be free of sulfur, carbon, and oxygen impurities.

The crystal could be cooled to 120 K with liquid nitrogen and heated to 1100 K by electron bombardment to the back of the crystal. A Chromel-Alumel thermocouple spot-welded to the back of the crystal was used to monitor the temperature. To minimize thermal drift the STM ramp housing the crystal and the STM scan head were allowed to thermally equilibrate for half an hour prior to STM measurements.

Separate XPS measurements were made in a second UHV system consisting of interconnected preparation and analysis chambers. The analysis chamber exhibited a base pressure of 2 × 10^{-10} Torr and was equipped with LEED optics, a Perkin-Elmer 04-548 dual anode X-ray source, an EA-10-plus hemispherical energy analyzer from SPECS, and a UTI 100c quadrupole mass spectrometer (QMS). The surface composition was probed with XPS, using nonmonochromatic Mg Kα X-rays. The photoelectrons were collected at the surface normal by the energy analyzer utilizing a 25 eV pass energy. Binding energies were calibrated with respect to the Au 4f peak (84.00 eV) and referenced to the Ni($2p_{3/2}$) peak. The preparation chamber reached a base pressure of 8 × 10^{-10} Torr and was equipped with a sputter ion gun and stainless steel gas dosers. The two chambers were isolated from each other during experiments. In the XPS system the crystal was heated resistively via two W wires spot-welded to the back of the crystal. The temperature was monitored by a Chromel-Alumel thermocouple spot-welded to the back edge of the crystal. The surface was cleaned by two Ar^+ sputter (500 eV, 1.5−2 μA, 300−500 K, 10 min) and anneal (1050 K, 10 min) cycles. Residual carbon was titrated away via oxygen treatment at 600 K. Within detectable limits, XPS showed the surface to be devoid of sulfur, carbon, and oxygen impurities following the cleaning procedure.

The purities of D_2S(g) (Cambridge Isotope Laboratories, 98%), O_2(g) (Praxair, 99.999%), CH_3OH(l) (Aldrich, 99.93%), CH_3CH_2OH(l) (Aldrich, 99.5%), $CH_3CH_2CH_2OH$(l) (Fluka, 99.8%), and C_6H_5OH(s) (Aldrich, 99%) were monitored with the QMS during dosing. All gases were introduced from a needle doser directed at the surface with the opening 1 in. from the surface of the crystal. Uncorrected exposures determined from background partial pressures are reported in units of Langmuir (1 L = 10^{-6} Torr s). The alcohols were routinely purified under vacuum by freeze−pump−thaw cycles until a constant vapor pressure was obtained over the solid.

The sulfur overlayer at the indicated coverages was generated via D_2S exposure at 300 K followed by heating (1 K/s) to 500 K and immediate quenching to 300 K. However, no significant

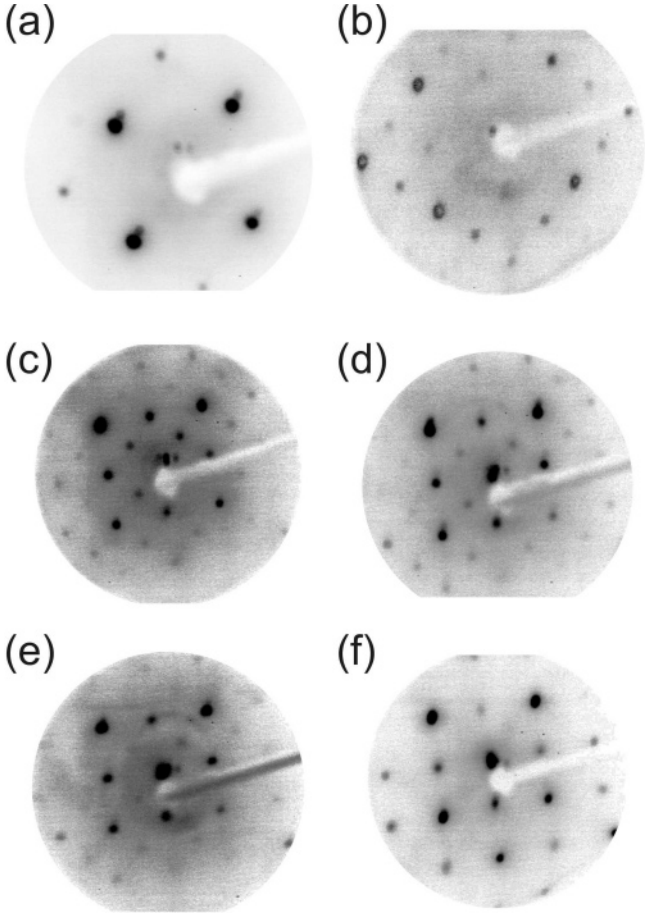

Figure 2. LEED patterns obtained following (a) our cleaning procedure and exposures to D_2S(g) (1×10^{-8} Torr) of (b) 1, (c) 2, (c) 5, (d) 10, (e) 20, and (f) 30 L at 300 K and annealing (1 K/s) to 500 K. The data were obtained at 300 K at 140−150 eV beam energies.

changes to the surface structure were observed without annealing to 500 K. Sulfur coverages were determined locally via STM.

A combination of STM and AES was used to calculate sulfur coverages. The sulfur coverage at 0.43 ML was calculated with STM and used to extrapolate to other coverages, using AES and the following relationship:

$$\theta\,(\mathrm{ML}) = [(S_{152\ \mathrm{eV}}/Ni_{848\ \mathrm{eV}})_\theta/(S_{152\ \mathrm{eV}}/Ni_{848\ \mathrm{eV}})_{0.43\ \mathrm{ML}}] \times 0.43\ \mathrm{ML} \quad (3)$$

$S_{152\ eV}$ is the peak-to-peak height of the sulfur AES signal at 152 eV and $Ni_{848\ eV}$ is that of Ni at 848 eV. Coverages determined with eq 3 were found to be in good agreement with those estimated with STM measurements.

C. Results and Discussion

C.1. The Sulfur Adlayer. LEED patterns for adsorbed sulfur observed here were consistent with those observed previously (Figure 2). The diffraction patterns evolved from (1×1) to $p(2 \times 2)$ to $c(2 \times 2)$ with increasing sulfur coverage. Exposure of the clean surface (Figure 2a) to 1.0 L of D_2S effected the appearance of faint $p(2 \times 2)$ spots (Figure 2b). The center spot in the $p(2 \times 2)$ diffraction pattern grew in intensity upon further D_2S exposure, eventually yielding a sharp $c(2 \times 2)$ LEED pattern (Figure 2f) at saturation coverage. LEED patterns such as those reproduced in Figure 2 have been used to suggest equivalent, real-space surface structures.[3,9] The $p(2 \times 2)$ and $c(2 \times 2)$ structures correspond to local sulfur coverages of 0.25 and 0.5 ML, respectively. Previous investigators have suggested

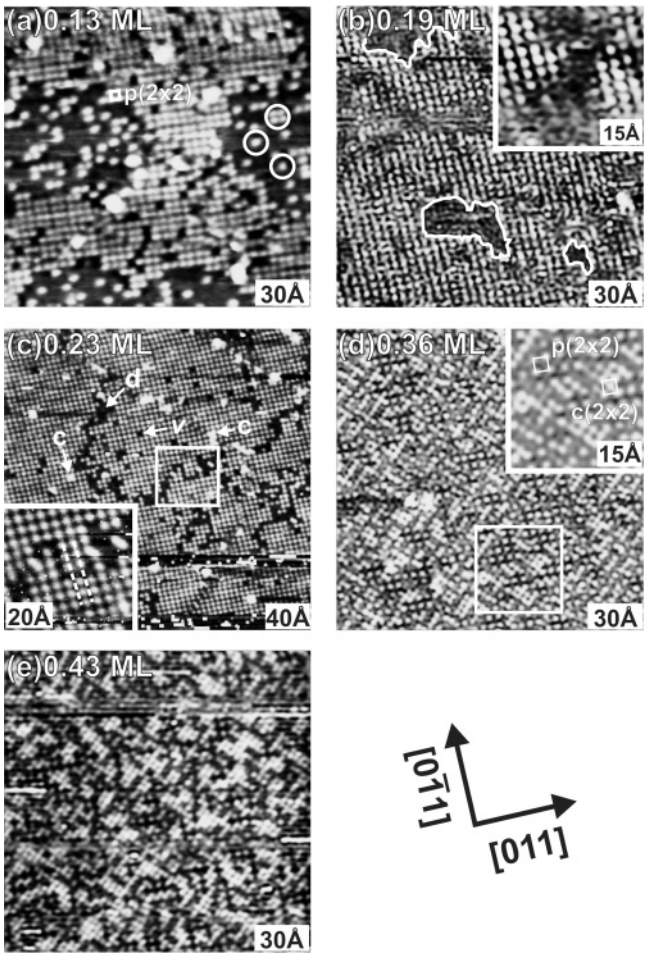

Figure 3. STM images showing the evolution of the sulfur-covered surface with increasing coverage. All images were obtained under constant height mode; coverages and tunneling conditions were the following: (a) 0.13 ML, −98.6 mV, 1.00 nA, the white circles denote atoms in a $p(2 \times 2)$ arrangement; (b) 0.19 ML, −0.51 V, 0.64 nA, and inset, −334 mV, 0.74 nA; (c) 0.23 ML, −179 mV, 0.90 nA, and inset, −179 mV, 0.87 nA; (d) 0.36 ML, −434 mV, 1.06 nA; (e) 0.43 ML, −439 mV, 0.83 nA. The insets to panels c and d are enlargements of the boxed areas. Scattered clusters of sulfur atoms, as well as isolated adatoms, have been indicated in panel a by open circles. Surfaces were prepared by exposures to D_2S(g) of (a) 1, (b) 2, (c) 5, (d) 10, and (e) 30 L followed by annealing to 500 K.

that between these intermediate sulfur coverages, the surface structure is characterized by domains of $p(2 \times 2)$ and $c(2 \times 2)$,[9] though details of the structure of the domain boundaries have not been reported.

STM scans of the surface show the evolution of the sulfur overlayer with increasing sulfur coverage (Figure 3). The state of the surface at low sulfur coverage consists of patches of the $p(2 \times 2)$ structure amid regions of clean surface (Figure 3a). The LEED pattern observed in this case showed clear $p(2 \times 2)$ features (Figure 2b). The unit cell consists of sulfur atoms spaced two lattice unit vectors along the [011] and [0$\bar{1}$1], giving a $p(2 \times 2)$ structure. Scattered, immobile clusters of sulfur atoms in local $p(2 \times 2)$ arrangements as well as isolated adatoms also appear on the surface (white circles).

With increasing sulfur coverage the domains of sulfur grew, while areas of the clean surface shrank (Figure 3b). Patches typical of the remaining uncovered surface are encircled by white borders. At a sulfur coverage of 0.23 ML (Figure 3c) the surface consisted of domains of the $p(2 \times 2)$ structure, domain boundaries (arrow d), and numerous vacancies (arrow v). Additionally, there were patches of $c(2 \times 2)$-S (arrow c). The

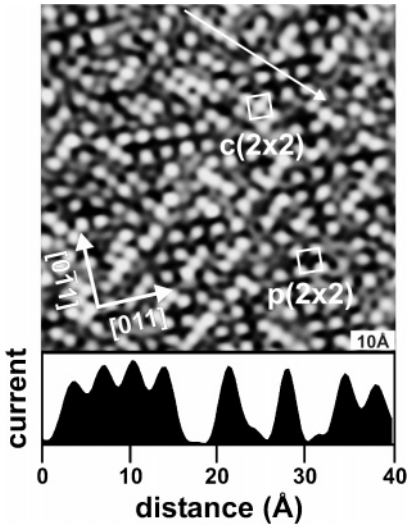

Figure 4. STM image and accompanying line scans of a sulfur-covered surface; tunneling conditions: −434 mV, 1.02 nA (constant height). The sulfur coverage is estimated to be 0.38 ML.

coverage of vacancies is approximately 0.02 ML. Atoms comprising the p(2 × 2) structure on one side of the domain boundary are offset by one lattice unit vector in the [0$\bar{1}$1] or [011] direction from those on the opposite side of the domain boundary (Figure 3c, inset). The distribution of sulfur atoms and domain boundaries suggests that the sulfur overlayer evolves via the nucleation and growth at multiple sites on the surface.

A further increase in sulfur coverage affected the appearance of the c(2 × 2) sulfur structure (0.36 ML, Figure 3d). The sulfur atoms appear to rearrange to yield a surface structure devoid of domain boundaries. Atoms of sulfur appear to add in a chainlike fashion between sulfur atoms in the p(2 × 2) structure along the [010] and [001] azimuths to give linked, localized c(2 × 2) patches running along these directions. At higher coverages the c(2 × 2) patches grew in size (Figure 3e).

Line scans across domains of the p(2 × 2) and c(2 × 2) structures (Figure 4) indicate that the atoms that comprise these moieties are electronically identical, as expected if they are all sulfur atoms. The line scan was taken across unit cells that consisted of both the p(2 × 2) and c(2 × 2) sulfur structures. A two-dimensional model consistent with the structures observed in this work is shown in Figure 5. The model surface is comprised of domains of the p(2 × 2) and c(2 × 2) structures, and localized c(2 × 2) structures between p(2 × 2) domains (Figure 5, arrow c).

The evolution of the sulfur-covered surface is in agreement with previous TPD and LEED studies.[17] In that study changes in the distribution of desorption states produced by coadsorbed $C^{16}O$ and $C^{18}O$ adlayers on sulfur-precovered Ni(100) were probed. At various sulfur coverages, $C^{16}O$ and $C^{18}O$ were adsorbed sequentially and the distribution of the isotopes desorbing from the different binding states on this surface was observed. At low sulfur coverages, the distribution of $C^{16}O$ and $C^{18}O$ showed complete interstate mixing of isotopes. At higher coverages $C^{16}O$ and $C^{18}O$ evolved from the states into which they were initially adsorbed; there was no interstate mixing.

Measurements of this nature were used to assess the distribution of p(2 × 2) and c(2 × 2) sulfur structures on surfaces that yielded the respective TPD spectra. Below 0.2 ML of sulfur coverage the sulfur atoms were predominantly clustered into islands of the p(2 × 2) structure. Between $\theta_s = 0.31$ ML and $\theta_s = 0.45$ ML, interstate mixing was hindered, indicating that

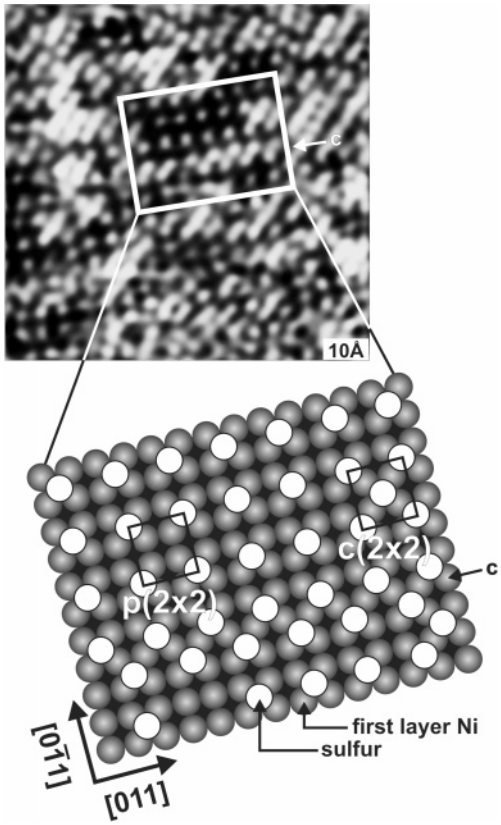

Figure 5. STM scan and two-dimensional model showing the p(2 × 2) and c(2 × 2) sulfur structures, and atoms of sulfur in a c(2 × 2) arrangement between p(2 × 2) domains (arrow c).

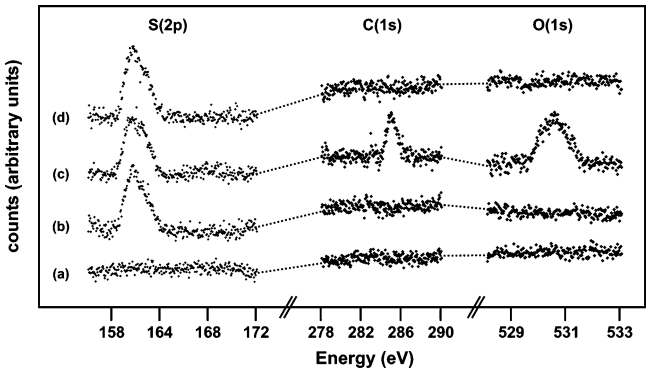

Figure 6. XPS spectra of (a) the clean Ni(100) surface, (b) the clean surface at 300 K following exposure to D_2S(g), annealing to 500 K, and quenching to 300 K, (c) the surface in part b after exposure to methanol, and (d) the surface in part d following annealing to 900 K. All of the spectra were obtained at 300 K.

the sulfur adlayer consisted of domains of the p(2 × 2) and c(2 × 2) structures.

C.2. Alkoxide Adsorption on the Sulfur-Covered Surface. *C.2.1. X-ray Photoelectron Spectroscopy.* X-ray photoelectron spectroscopy (XPS) scans of the Ni(100)-p(2 × 2)-S during methoxy adsorption are shown in Figure 6. The surface following cleaning was devoid of carbon, oxygen, and sulfur-containing impurities (Figure 6a). This surface was exposed to D_2S(g) to adsorb sulfur and flashed to 500 K. The resulting surface displayed a p(2 × 2) LEED pattern. The XPS spectrum of this surface consisted of S(2p) doublets (Figure 6b) with S($2p_{3/2}$) core energy (161.7 eV) consistent with what is expected for atomic sulfur.[18] The D_2S(g) exposure was sufficient to generate a sulfur overlayer at approximately 0.23 ML of coverage, as determined by STM previously (Figure 3c).

Exposure of the p(2 × 2) sulfur-covered surface to methanol gave a surface intermediate displaying C(1s) and O(1s) peaks at 285.0 and 530.6 eV, respectively (Figure 6c). From the ratio of carbon and oxygen photoionization cross sections (0.35),[19] the ratio of carbon and oxygen peak areas is 0.9, or approximately 1, which is consistent with a methoxy (CH_3O) surface intermediate. From the C(1s) and S(2p) peak areas, the ratio of carbon and sulfur photoinozation cross sections (0.57), and the sulfur coverage (0.23 ML), the carbon coverage is 0.04 ML. Annealing the surface to 900 K desorbed methoxy, giving the sulfur-covered surface (Figure 6d).

The carbon coverage following methoxy adsorption is close to the coverage of p(2 × 2)-S vacancies determined via STM (0.02 ML), which suggests that the vacancies are sites of methoxy adsorption.

C.2.2. Methoxy, Ethoxy, 1-Propoxy, and Phenoxy Adsorption. The adsorption of methanol, ethanol, 1-propanol, and phenol on the sulfur-covered Ni(100) surface was investigated at low (0.13 ML), medium (0.23 ML), and high (0.43 ML) sulfur coverages with STM. Changes to the surface electronic structure (i.e. corrugation) following alkoxide formation were observed at sulfur coverages at 0.23 ML only, presumably due to the mobility of the alkoxide at lower sulfur coverage and the absence of available sites at the highest sulfur coverage. Since the electronic corrugation is a function of the local density of states (LDOS), these changes were ascribed to alkoxy formation. The initial condition of the surface at 0.23 ML of sulfur coverage is shown in Figure 7a. It consisted of the p(2 × 2)-S structure, scattered p(2 × 2)-S vacancies (*v*), and sites one lattice unit along the [011] and [01$\bar{1}$] directions from sulfur atoms in the p(2 × 2) structure (in-between hollows, *i*). Exposure of this surface to methanol, ethanol, 1-propanol, and phenol (ROH) affected changes to the electronic corrugation at the p(2 × 2) vacancies (Figure 7b−e). These changes are clearly seen in line scans taken across the vacancies (Figure 8). The line scan taken across a vacancy prior to ROH exposure (Figure 8a) became deeper after methoxy adsorption (Figure 8b), while protrusions were observed following ethoxy (Figure 8c), 1-propoxy (Figure 8d), and phenoxy (Figure 8e) adsorption. Clearly these vacancies serve as binding sites for the alkoxides. Additionally, phenoxy appears to adsorb into in-between hollow sites (Figure 9).

Heating the methoxy covered p(2 × 2)-S surface to 500 K restored the vacancies to their initially unoccupied state. Changes to the depths of the vacancies—taken as difference between sulfur peaks and vacancy depths—following methoxy adsorption and desorption are depicted by column plots (Figure 10). The data were averaged over several STM images. The corrugation across sulfur atoms in the p(2 × 2) structure was approximately the same in each image (within 5%), indicating that the tip and tunneling conditions were similar, enabling direct comparison of the line scans. As expected, the corrugation across sulfur and the clean, uncovered surface (Figure 10a) was similar to that across the p(2 × 2)-S vacancies prior to methanol exposure (Figure 10b). The latter became deeper following methoxy adsorption (Figure 10c). Annealing this surface to 500 K (cf. eq 2) returned the vacancy electronic structure to its initially unoccupied state (Figure 10d).

The binding sites observed following RO− adsorption onto the Ni(100)-p(2 × 2)-S covered surface are summarized in the two-dimensional model shown in Figure 11. Occupation of in-between hollows was observed for phenoxy only; no changes in the electronic corrugation were observed across the in-between hollows following the adsorption of methoxy, ethoxy, and 1-propoxy.

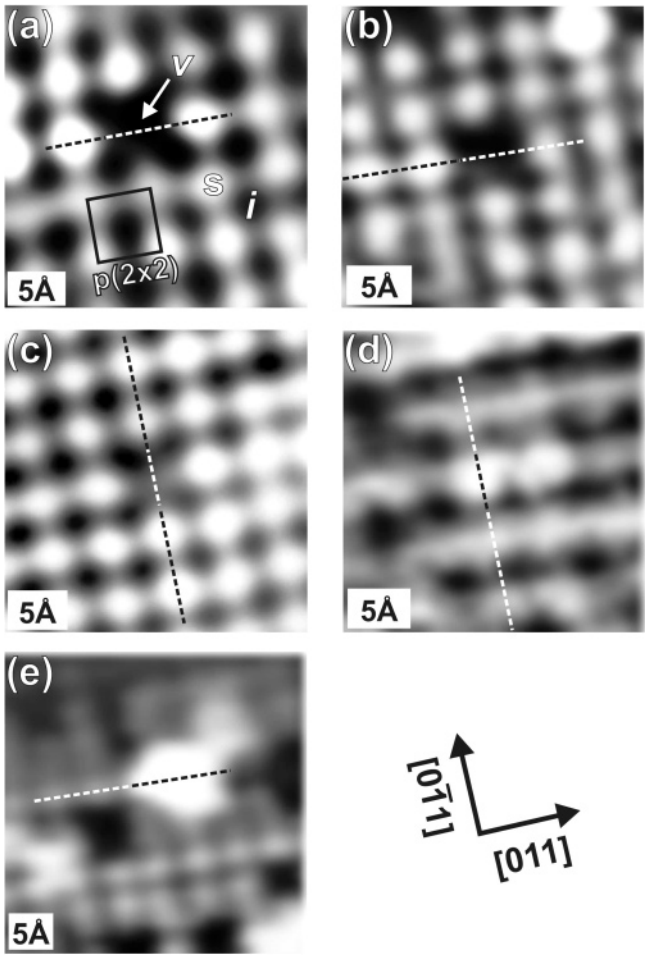

Figure 7. Constant height STM micrographs of the (a) 0.23 ML sulfur covered Ni(100) surface following exposure to (b) CH_3OH(g), (c) CH_3CH_2OH(g), (d) $CH_3CH_2CH_2OH$(g), and (e) C_6H_5OH(g); tunneling conditions: (a) 1.0 mV, 0.60 nA; (b) 129.0 mV, 1.04 nA; (c) −11.9 mV, 1.12 nA; (d) −2.1 V, 0.75 nA; and (e) −2.0 V, 0.95 nA. A p(2 × 2)-S vacancy (*v*) and an in-between hollow site (*i*) have been indicated in panel a. The corrugation across the sulfur atoms is approximately 0.4 nA. Line scans (dashed lines) across surface features are shown in Figure 8.

C.2.3. Selective Poisoning. Adsorption of methoxy, ethoxy, 1-propoxoy, and allyl alkoxy on the Ni(100) surface at θ_s < 0.2 ML did not affect changes to the distribution of sulfur atoms or the electronic structure of features associated with the sulfur adlayer. The surface at sulfur coverage below 0.2 ML consisted of p(2 × 2)-S domains and the clean surface. No changes to the surface structure were observed following ROH exposure. Similarly, the sulfur-covered surface at θ_s > 0.35 ML was generally stable toward ROH (methanol and ethanol) exposure. At these sulfur coverages the density of vacancies is significantly lower than at 0.23 ML of sulfur coverage. These results are in agreement with the adsorption of the alkoxy into p(2 × 2)-S vacancies.

XPS and STM results are suggestive of the p(2 × 2) vacancies being the active sites for selective poisoning. Changes to the vacancy electronic structure following ROH exposure to the 0.23 ML of sulfur covered surfaces—coupled with the equality between the methoxy and p(2 × 2)-S vacancy coverages—suggests that the alkoxy surface intermediates adsorb in p(2 × 2)-S vacancies. Noting the changes to the electronic corrugation, particularly those following methoxy adsorption and decomposition with heating (Figure 8), results suggest that the 4-fold hollow vacancies are the active sites for selective

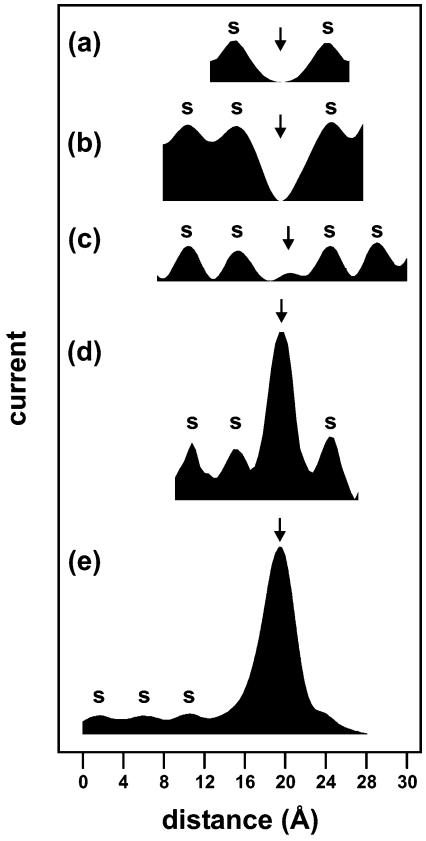

Figure 8. Line scans taken across vacancies in the direction of the [011] or [011] surface vectors of the STM images in Figure 7. Atoms of sulfur (S) and vacancy positions (vertical arrows) have been indicated. The corrugation across the sulfur atoms is approximately 0.4 nA.

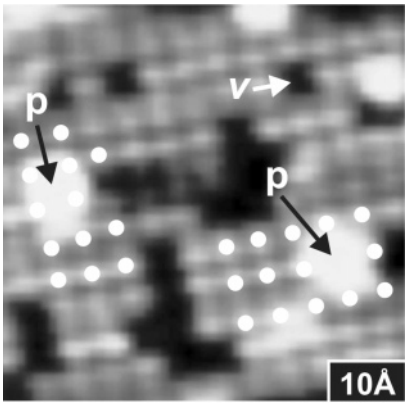

Figure 9. An enlargement of Figure 6e showing phenoxy (arrow p) and vacancies (arrow v) amid the p(2 × 2)-S structure; tunneling conditions: −2.0 V, 0.95 nA. The white circles accentuate the positions of select sulfur atoms.

poisoning. These results are partially consistent with what was originally posited by Madix et al., who suggested that the c(2 × 2) vacancies were the active sites for selective poisoning.[9]

D. Summary

STM and LEED have been used to probe the sulfur-covered Ni(100) surface with increasing coverage. The STM images reveal details of the p(2 × 2) and c(2 × 2) sulfur structures. At low sulfur coverage STM measurements reveal the surface to be partially covered by islands of p(2 × 2)-S. With increasing sulfur coverage p(2 × 2) domains of sulfur grow in size, until the surface is largely covered by p(2 × 2)-S with numerous domain boundaries, vacancies, and scattered domains of sulfur in a c(2 × 2) arrangement. With further sulfur adsorption the high coverage c(2 × 2)-S dominates the surface structure. Patches of the p(2 × 2) at low sulfur coverage and domain boundaries between islands of p(2 × 2)-S at higher coverages are suggestive of nucleation and growth at multiple sites on the surface. At sulfur coverages approaching 0.25 ML the domain boundaries disappear, suggesting a rearrangement of the sulfur adatoms to yield an optimized overlayer. Upon further sulfur adsorption, the overall driving force to form the c(2 × 2) structure exceeds sulfur−sulfur repulsive interactions and c(2 × 2) domains grow in size.

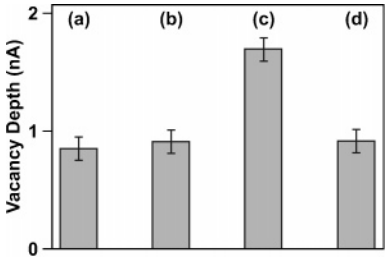

Figure 10. Column plots of measured vacancy depths (sulfur peak to vacancy trough) on the following surfaces: (a) sulfur and the clean, uncovered surface, (b) p(2 × 2)-S vacancies, (c) p(2 × 2)-S vacancies following CH_3OH(g) exposure, and (d) p(2 × 2)-S vacancies in part c after heating the surface to 500 K to decompose CH_3O.

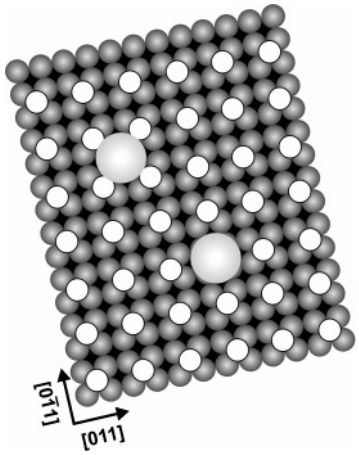

Figure 11. Two-dimensional model showing the adsorption sites of the surface intermediates following exposure of the p(2 × 2)-S covered surface to CH_3OH(g), CH_3CH_2OH(g), $CH_3CH_2CH_2OH$(g), and C_6H_5OH(g). Adsorption into the in-between hollow sites was observed for phenoxy only.

Methoxy, ethoxy, and 1-propoxy adsorb into p(2 × 2)-S vacancies. Phenoxy adsorbs into p(2 × 2)-S vacancies and in-between hollows. The p(2 × 2)-S vacancies are believed to be the sites for adsorption of the alkoxides and the active sites for the partial dehydrogenation of the surface intermediates.

Acknowledgment. We are grateful to the National Science Foundation (NSF CHE 0209546) for support of this work.

References and Notes

(1) Besenbacher, F.; Stensgaard, I.; Ruan, L.; Norskov, J. K.; Jacobsen, K. W. *Surf. Sci.* **1992**, **272**, 334.

(2) Carley, A. F.; Davies, P. R.; Jones, R. V.; Harikumar, K. R.; Kulkarni, G. U.; Roberts, M. W. *Surf. Sci.* **2000**, *447*, 39.

(3) Perdereau, M.; Oudar, J. *Surf. Sci.* **1970**, *20*, 80.

(4) Brennan, S.; Stohr, J.; Jaeger, R. *Phys. Rev. B* **1981**, *24*, 4871.

(5) Duke, C. B.; Lipari, N. O.; Laramore, G. E.; Theeten, J. B. *Solid State Commun.* **1973**, *13*, 579.

(6) Partridge, A.; Tatlock, G. J.; Leibsle, F. M.; Flipse, C. F. J. *Phys. Rev. B* **1993**, *48*, 8267.
(7) Partridge, A.; Tatlock, G. J.; Leibsle, F. M. *Surf. Sci.* **1997**, *381*, 92.
(8) Johnson, S.; Madix, R. J. *Surf. Sci.* **1981**, *103*, 361.
(9) Madix, R. J.; Lee, S. B.; Thornburg, M. *J. Vac. Sci. Technol. A* **1982**, *1*, 1254.
(10) Johnson, S. W.; Madix, R. J. *Surf. Sci.* **1982**, *115*, 61.
(11) Gland, J. L.; Madix, R. J.; McCabe, R. W.; Dimaggio, C. *Surf. Sci.* **1984**, *143*, 46.
(12) Vasquez, N.; Muscat, A.; Madix, R. J. *Surf. Sci.* **1995**, *339*, 29.
(13) Huberty, J.; Madix, R. J. *Surf. Sci*. **1996**, *360*, 144.
(14) Huberty, J.; Madix, R. *Surf. Sci.* **1995**, *334*, 77.
(15) Crew, W. W.; Madix, R. *Rev. Sci. Instrum.* **1995**, *66*, 4552.
(16) Besenbacher, F.; Stensgaard, I. In *The Chemical Physics of Solid Surfaces*; King, D. A., Woodruff, D. P., Eds.; Elsevier Science Publishers: New York, 1993; Chapter 15.
(17) Muscat, A. J. In *Chemical Engineering*; Stanford University: Stanford, CA, 1992; p 379.
(18) Alemozafar, A. R.; Guo, X.-C.; Madix, R. J. *J. Chem. Phys*. **2002**, *116*, 4698.
(19) Scofield, J. H. *J. Electron Spectrosc*. **1976**, 8, 129.